Research Article

Duygu Sen Baykal*

A comparative investigation of neutron and gamma radiation interaction properties of zircaloy-2 and zircaloy-4 with consideration of mechanical properties

https://doi.org/10.1515/phys-2024-0088
received June 04, 2024; accepted September 17, 2024

Abstract: This study has established the radiation shielding efficacy of zircaloy-2 and zircaloy-4 over a wide spectrum of energy levels. Using the Monte Carlo method, the gamma and neutron transmission factors (TF and nTF) were calculated for various energy levels. Zircaloy-2 demonstrated the highest gamma-ray absorption capacity and the lowest neutron absorption capacity among the investigated alloys. The results indicate that zircaloy-2 and zircaloy-4 have nearly the same neutron transmission characteristics. Although many studies have examined the structure and physical characteristics of these materials, there has been a lack of Monte Carlo simulations to comprehensively investigate the correlation between gamma absorption, neutron absorption parameters, and mechanical qualities. This research aims to examine the ability of zirconium and its zircaloy-2 and zircaloy-4 alloys, which are critical materials used in the nuclear industry, to absorb gamma and neutron radiation over a broad spectrum of frequencies. According to the results, zircaloy-2 has the best ability to absorb secondary gamma rays and the highest level of resistance to them. Despite the minimal disparity in the nTF between the two alloys, simulation results have shown that zircaloy-2 has a higher level of neutron transmittance. These results have the potential to expedite the development of novel materials with enhanced attributes for various applications.

Keywords: zirconium alloys, zircaloy-2, zircaloy-4

*** Corresponding author: Duygu Sen Baykal**, Faculty of Engineering and Architecture, Mechatronics Engineering, Istanbul Nisantasi University, 34398, Istanbul, Turkey,
e-mail: duygu.senbaykal@nisantasi.edu.tr

1 Introduction

Zirconium, a transition metal belonging to group four of the periodic table, undergoes phase transitions in response to varying circumstances such as temperature and pressure. These modifications lead to the acquisition of distinct crystal structures in their solid states. Zirconium undergoes a phase transition to its high-temperature phase when the temperature is above 1,139 K [1,2]. These phase transitions are crucial as they significantly affect the metal's mechanical properties and its behavior in many scenarios. Radiation is the process by which energy is emitted from a source and can propagate through empty space, with the ability to penetrate various materials. The interaction between radiation and materials is crucial for understanding their ability to shield against radiation and their effectiveness in protecting against radiation hazards [3]. The use of high-energy ionizing radiations, especially gamma rays, is rapidly growing in many sectors, such as industries, medical diagnostics, and nuclear research. Inadvertent exposure to gamma rays, which possess a highly energetic and penetrating nature, is of great concern due to their detrimental effects on human health, including radiation sickness and cancer. Understanding the shielding effectiveness of materials against gamma rays is essential for developing protective measures in these fields [4,5]. Zirconium alloys have many beneficial attributes, including a low thermal neutron capture cross-section, acceptable mechanical qualities, and excellent corrosion resistance [6–8]. Zirconium and its alloys are extensively used in many contemporary technologies, especially in the medical sector, due to their advantageous characteristics. The use of zirconium is enhanced in these domains due to its resistance to corrosion in severe environments, compatibility with biological systems, stability at elevated temperatures, and low propensity to absorb thermal neutrons [9]. These properties

make zirconium an ideal material for various applications, including those that involve high levels of radiation. Radiopharmaceutical chemicals are often used in nuclear medicine imaging equipment, such as gamma cameras and positron emission tomography scanners. Zirconium is the ideal material for creating these devices because of its excellent strength and resistance to radiation. Furthermore, the equipment necessary for the manufacturing of radiopharmaceutical agents is constructed using materials that possess a significant level of resistance to both corrosion and radiation. When constructing the structural components of these devices, it is essential to use materials that are resistant to long-term radiation exposure and possess a high level of mechanical strength [10–13]. Hence, it is essential to assess the durability of materials against gamma and neutron radiation in this particular scenario. Zircaloy is a mostly zirconium-based alloy, often consisting of 95–98% zirconium, in addition to tiny amounts of other metallic elements. Zircaloy-2 is primarily composed of 98% zirconium, with additional amounts of tin (ranging from 1.2 to 1.7%), iron (ranging from 0.07 to 0.2%), chromium (ranging from 0.05 to 0.15%), and nickel (ranging from 0.03 to 0.08%). Zircaloy-4 exhibits similarities, but with minor discrepancies in the proportions of iron and chromium. Understanding the composition and properties of these alloys is crucial for evaluating their performance under radiation exposure. This research aims to examine the ability of zirconium and its zircaloy-2 and zircaloy-4 alloys, which are critical materials used in the nuclear industry, to absorb gamma and neutron radiation over a broad spectrum of frequencies. To optimize the use of zirconium and its derivatives, such as zircaloy-2 and zircaloy-4, in future technologies like high-entropy alloys and other zirconium-based alloys, it is imperative to enhance our understanding of their present characteristics.

2 Materials and methods

2.1 Monte Carlo simulations of investigated alloy samples

The utilization of Monte Carlo simulation holds great significance in the realm of radiation transport investigations. Monte Carlo simulations utilize random sampling to model and analyze the interaction between radiation and matter, rendering them a potent computational tool. Monte Carlo simulation plays a pivotal role in this domain due to several significant factors. Additionally, it allows for an accurate depiction of intricate radiation interactions and transport, considering diverse factors such as particle categorization, energy level, scattering features, and absorption characteristics. The role of geometry in the Monte Carlo method is of utmost importance in computer modeling and simulation, as it directly impacts the accuracy, efficiency, and applicability of simulations across various domains. The precision of geometric depiction is crucial, as it directly affects the probability of particle interactions, scattering occurrences, and the overall movement of energy and matter in the system. The Monte Carlo method is renowned for its capacity to efficiently tackle intricate issues through the utilization of random sampling. However, in order to yield appropriate outcomes, it necessitates a precise depiction of geometric structures and bounds. The Monte Carlo approach models system behavior by tracing the paths and interactions of particles within a specified geometric area [14]. This space encompasses the limits, substances, and arrangements that are relevant to the matter being examined. Precise geometric modeling is crucial for accurately predicting the absorption and deflection of radiation in various materials and barriers. A further pivotal factor in Monte Carlo simulations, specifically in Monte Carlo N-Particle simulation code, is the precise depiction of the system's geometry. Geometry is crucial in establishing the trajectories that particles follow and, as a result, their interactions inside the material. Simulation outcomes can be significantly affected by an inaccurate geometric arrangement. Hence, it is crucial to provide a thorough and precise characterization of geometric features, encompassing shapes, sizes, and spatial arrangement in order to accurately replicate real-world circumstances in simulated interactions. The accuracy of the simulation results is improved by this precision. Precise geometric modeling enables precise calculation of radiation shielding, material testing, and other crucial characteristics [15]. Monte Carlo methods offer comprehensive and authentic depictions of radiation transport phenomena by means of simulating a considerable number of particle histories. It is noteworthy that Monte Carlo N-Particle code [16–18] is a tool of great flexibility and potency, albeit necessitating a profound comprehension of the fundamental physics and meticulousness in configuring the simulation. To establish the geometric properties of a given system, it is necessary to identify and analyze the constituent elements, such as the source, target, and any other pertinent components. The structural design may range from a basic monolithic slab to a sophisticated multi-tiered configuration. Allocate suitable materials to every constituent in geometric structure is significant. Therefore, providing a comprehensive description of the

Table 1: Investigated alloy types, elemental mass fractions (wt%), and material densities (g/cm^3)

Sample	Zr	Sn	O	Fe	Cr	Ni	Density
Zirconium	100	—	—	—	—	—	6.53
Zircaloy-2	98.23	1.4	0.12	0.10	0.10	0.050	6.56
Zircaloy-4	98.18	1.4	0.12	0.20	0.10	—	6.56

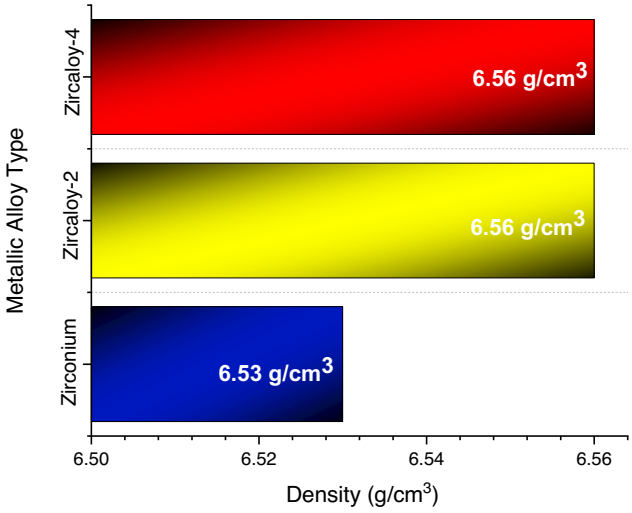

Figure 1: Variation of investigated metallic alloy densities.

Table 2: Mechanical properties of the investigated alloys [19]

Mechanical Properties	Metric		
	Zirconium	Zircaloy-2	Zircaloy-4
Tensile strength, ultimate	330 MPa	≥413 MPa	Min 413 MPa
Tensile strength, yield	230 MPa	≥241 MPa	Min 241 MPa
Elongation at break	32%	20%	20%
Modulus of elasticity	94.5 GPa	99.3 GPa	99.3 GPa
Poisson's ratio	0.34	0.37	0.37
Shear modulus	35.3 GPa	36.2 GPa	36.2 GPa

materials' composition (Table 1), density (Figure 1), and pertinent characteristics are significant actions during the preparation of the input file. Additionally, their mechanical properties as found in the literature (Table 2) [19]. In this study, geometry was considered a structural design of the material under investigation. Figure 2 depicts the modelled with the 2D and 3D images obtained from the visual editor. The related materials have been carefully inserted into the data card section of the input file. The used materials were separately prepared through the M_n feature of the Monte Carlo N-Particle code. The term source refers to the origin or starting point of something, such as information, data, or a product [20,21]. The Monte Carlo N-Particle code provides a range of source alternatives, such as point sources, isotropic sources, and intricate source distributions. In this study, gamma-ray and neutron transmission factors (TF) were separately investigated using two different source definitions. During the initial phase of the study, we examined the values of gamma-ray TFs. Particularly, this investigation focused on three distinct radioisotope energies – 0.662, 1.1732, and 1.3325 MeV – which are emitted from ^{137}Cs and ^{60}Co and were utilized as point isotropic radiation sources. The simulation geometry was meticulously established to ensure a precise depiction of the material's size and boundary conditions, while employing suitable energy spectra to accurately reflect the emission properties of the radioisotopes. During the second phase, the source geometry was modified to function as a neutron source that releases fast neutrons with an energy level of 2 MeV. This allowed us to expose the material to radiation and measure the amount of secondary radiation on the opposite side of the material. Tallies are employed as a means of gathering and analyzing data in Monte Carlo N-Particle simulations. It is recommended to establish a tally for the purpose of registering the particles or fluence that have been transmitted. Specify the suitable type of tally and place it within the area where the TF is to be computed. The study employed an F4 tally mesh to quantify the mean flux of both photons and neutrons. Two independent F4 tally meshes were created, one positioned in front and the other behind the material. Consequently, two F4 tally meshes yielded distinct results that were subsequently extracted from the output file for the purpose of calculating TFs. The present investigation aimed to optimize the simulation geometry to minimize the particle track process of the code, thereby enhancing simulation efficiency. Furthermore, the radiation type was identified in both simulations to eliminate superfluous tracking and enhance simulation efficiency. Upon completion input file, its executed the Monte Carlo N-Particle code utilizing our input file as the designated input. It's worth mentioning that Phy-X/PSD [22–27] code was also utilized for other fundamental gamma-ray shielding parameters such as attenuation coefficient, half value layer, and build-up factors.

2.2 Investigated shielding parameters for gamma ray and neutrons

The mass attenuation coefficient (MAC), represented by μ/ρ, is a metric that quantifies the degree to which a

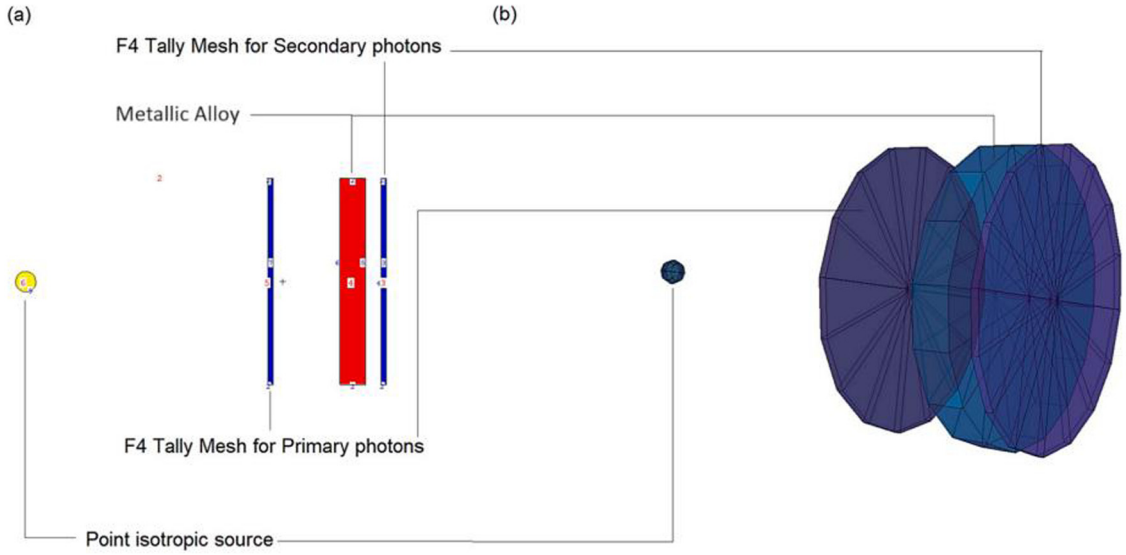

Figure 2: (a) 2D and (b) 3D illustrations of designed Monte Carlo simulation setup.

substance diminishes the intensity of a radiation beam during its traversal. The linear attenuation coefficient (μ) is divided by the material's density (ρ) to obtain its ratio, as seen in the formula [28]:

$$\mu_{\mathrm{m}} = \mu/\rho, \tag{1}$$

The determination of radiation attenuation in diverse materials is facilitated by the utilization of the MAC, which is frequently available in tables or databases for distinct radiation types (*e.g.*, X-rays or gamma rays) and materials. The half-value layer (HVL) is a metric that quantifies the quantity or thickness of a substance necessary to decrease the intensity of a radiation beam to 50% of its initial magnitude. The term HVL denotes the depth of a particular material at which the intensity of radiation is reduced by half as it traverses through it. The HVL formula is as follows [28]:

$$\mathrm{HVL} = \ln(2)/\mu, \tag{2}$$

where μ is the linear attenuation coefficient. The HVL is contingent upon the energy level of the radiation and the characteristics of the substance. The term is frequently employed to denote the capacity of materials to shield against radiation and is utilized in calculations pertaining to radiation protection. The term "mean free path" pertains to the typical distance traversed by a particle or photon within a given material prior to experiencing an interaction, such as absorption or scattering. The aforementioned is a statistical notion that denotes the mean distance separating consecutive interactions. The mfp formula is as follows [28]:

$$\mathrm{mfp} = 1/\mu. \tag{3}$$

The relationship between the mean free path and the linear attenuation coefficient (μ) of a material is inverse. Stated differently, it denotes the mean displacement that a particle can traverse prior to experiencing a substantial reduction in its energy. The Build-up Factor, commonly represented as B, is a correction factor utilized to consider the escalated radiation intensity that takes place beyond the HVL within a given material. The phenomenon of scattering and secondary radiation generated within a material during the passage of primary radiation is taken into account. The Energy Build-up Factor (EBF) and Energy Absorption Build-up Factor (EABF) formulas are as follows [29]:

$$\mathrm{EBF} = \frac{I_{\mathrm{total}}}{I_{\mathrm{Primary}}}, \tag{4}$$

$$\mathrm{EABF} = \frac{E_{\mathrm{total}}}{E_{\mathrm{Primary}}}, \tag{5}$$

where I_{total} and I_{Primary} are the total and primary intensities of radiation, and E_{total} and E_{Primary} are the total and primary energies of radiation, respectively.

The utilization of the build-up factor is crucial in the computation of the effective attenuation of radiation beyond the HVL. This factor plays a significant role in the determination of the comprehensive shielding prerequisites in the domain of radiation protection. The aforementioned terms are essential principles in the field of radiation physics and serve the purpose of defining and measuring the degree of radiation's interaction with matter. These play a pivotal role in various applications, including radiation therapy, radiology, nuclear

engineering, and radiation safety evaluations. The TF quantifies the proportion of radiation that traverses a given material without undergoing absorption or scattering. This factor is commonly presented in the form of a ratio or percentage and is computed using the following formula [30]:

$$\text{Transmission factor} = (\text{Number of transmitted particles}/\text{Number of incident particles}) \times 100, \quad (6)$$

where the "Number of transmitted particles" refers to the count of particles (neutrons or gamma rays) that pass through the material, and the "Number of incident particles" denotes the total number of particles that initially impinge upon the material. This formula is applicable to both neutrons and gamma rays, and it quantifies the ratio of particles that pass through the material. The configuration of the system, the material's composition and density, and the energy level of the particles all have an impact on the TF. Comprehending the TFs for both forms of radiation is essential for radiation shielding applications, as it aids in evaluating the efficacy of materials in reducing or permitting the passage of radiation. Monte Carlo simulations are frequently employed to calculate these variables and enhance shielding designs. The TFs for neutrons were found in this work using Monte Carlo N-Particle code simulations. Similarly, the same methodology can be employed to examine gamma rays, enabling a thorough evaluation of how radiation passes through different substances.

3 Results and discussions

3.1 Gamma-ray attenuation properties of investigated alloys

Radiation shielding is crucial in various applications such as nuclear power plants, medical facilities that use radiation, industrial radiography, and even space exploration. These applications require materials that can effectively reduce radiation exposure to ensure safety and functionality. The term MAC is important for radiation shielding because it provides a quantitative measure of how effectively a material attenuates or reduces the intensity of radiation as it passes through it. Understanding these coefficients is key to selecting the right materials for specific radiation environments. The investigated zirconium-based alloys' MACs' energy-dependent trend is depicted in Figure 3. The values of the MAC were highest at low energies. This is typically due to the increased interaction probability of low-energy photons with the material. As the energy increased and the MAC values moved into the intermediate energy range, they began to decline.

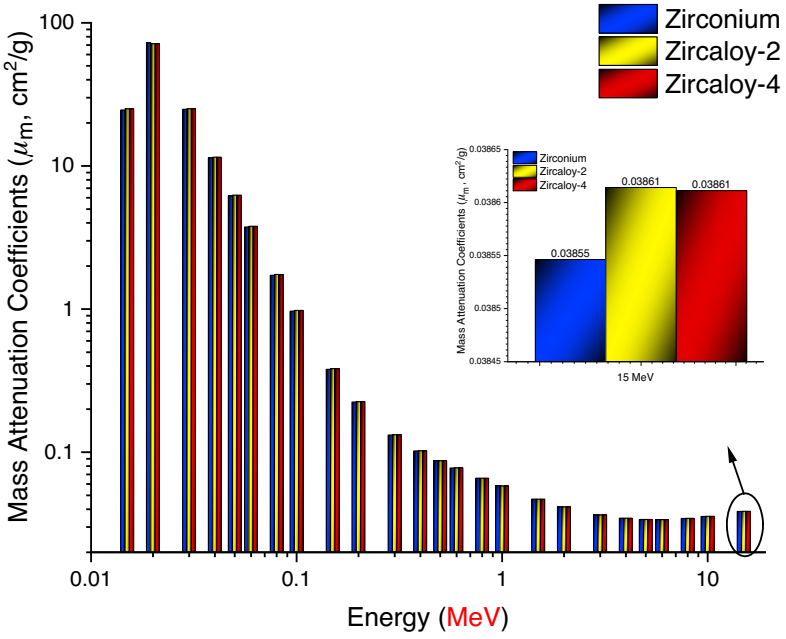

Figure 3: Variation of MACs (cm^2/g) with photon energy (MeV) for zirconium, zircaloy-2 and zircaloy-4.

This decline is attributed to the reduced probability of photoelectric absorption at higher energies. The MAC values reached their highest values in the high energy region, according to the changing trend in the figure. This increase at high energies can be linked to the predominance of pair production and other high-energy photon interactions. In this case, it can be observed that all three alloys stop low-energy photons quite effectively, but as energy increases, the values of the MACs of all three alloys decrease sequentially. In other words, when the gamma-ray energy increased, all three alloys exhibited behaviors that were identical to one another. The MACs of the alloys have, however, been found to vary, especially in the high-energy area. For instance, zircaloy-2 returned the greatest value for 15 MeV energy, followed by zircaloy-4 and pure zirconium, respectively. This indicates that zircaloy-2 is more effective at attenuating high-energy gamma rays, likely due to its unique alloying elements that enhance its shielding capabilities. The differences in the constituent composition of zircaloy-2 and zircaloy-4 alloys can be utilized to clarify this situation. The MACs parameter, as indicated in previous sections, is unrelated to density and has a direct correlation with the elemental compositions of the materials. These results, along with the differing chemical compositions of zircaloy-2 and zircaloy-4 alloys with the same density value, lead to different MAC values. The investigation analyzed the second parameter for radiation shielding competencies, which was the HVL. The HVL is a crucial parameter in comprehending the shielding characteristics of materials, as it denotes the thickness of the material required to reduce the primary beam quantity by half. The aforementioned quantity exhibits an inverse relationship with the linear attenuation coefficients. This relationship is critical for designing effective shielding, as it allows for the calculation of the material thickness needed to achieve the desired attenuation levels. Materials exhibiting high linear attenuation coefficients are anticipated to have low HVL values, in simpler terms. This phenomenon pertains to its exceptional absorption characteristics. The trend of variation of the HVL values for the three alloys under investigation across a broad energy spectrum is illustrated in Figure 4. The figure illustrates that low-energy photons yield low HVL (cm) values. This phenomenon occurs due to the susceptibility of low-energy photons with limited penetration capabilities to undergo attenuation even at extremely thin material depths. The HVL values exhibited a direct proportionality with the energy increment, resulting in an increase in the required values. The sample of zircaloy-2 exhibited the lowest HVL value, while the energy value of 15 MeV was found to be the highest. Zircaloy-2 is particularly effective at shielding against high-energy photons, which are more penetrating and thus require thicker materials for adequate attenuation. The relatively modest quantitative disparity between zircaloy-2 and zircaloy-4 can be attributed to the fact that the HVL is determined based on linear attenuation coefficients, which are directly proportional to density, despite the higher

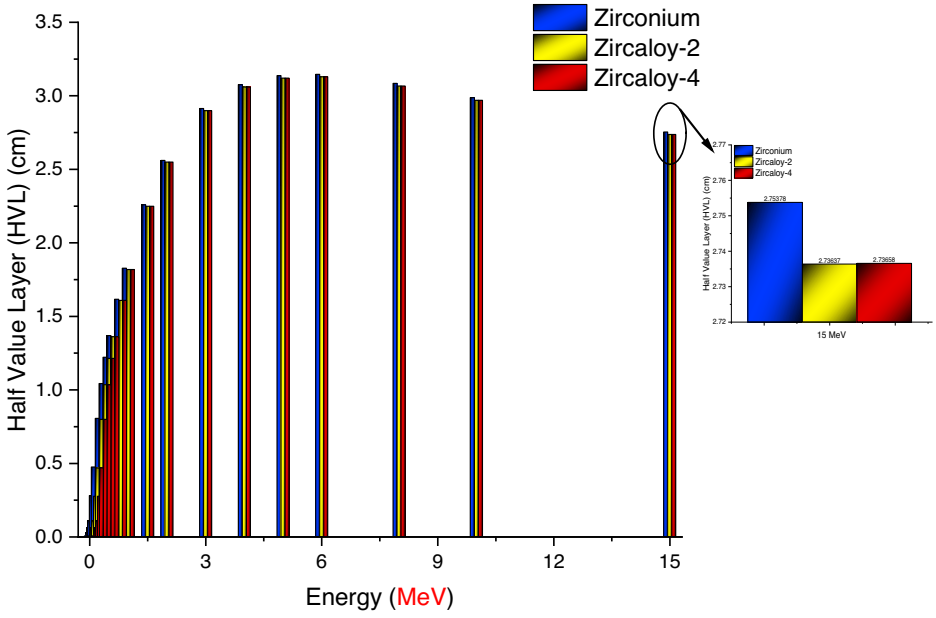

Figure 4: Variation of half value layer (cm) with photon energy (MeV) for zirconium, zircaloy-2 and zircaloy-4.

MACs observed in these materials. Therefore, while both alloys have similar densities, their different chemical compositions result in varying HVL values. Table 1 illustrates that despite both alloys possessing identical density values, there exists a discernible quantitative distinction between them. The quantitative disparity between the MACs of zircaloy-2 and zircaloy-4 is more evident when the density effect is disregarded, owing to the variations in their chemical configurations. These findings highlight the importance of considering both density and chemical composition when evaluating materials for radiation shielding. The notion of mean free path holds significant importance within the domain of radiation shielding. The term denotes the mean path length traversed by a particle, for instance, a photon or neutron, within a given medium prior to experiencing a collision. The comprehension of a material's efficacy in attenuating radiation within the realm of shielding materials is contingent upon the mean free path. As depicted in Figure 5, there is a positive correlation between energy and the average distance necessary for two successive interactions. This correlation is crucial for understanding how different energies of radiation interact with materials, which can influence the design of shielding systems. The phenomenon can be attributed to the correlation between the energy value and the distance traveled by energetic photons within the material. As the energy value increases, the photons tend to traverse a greater distance, leading to a subsequent increase in the distance between two consecutive interactions. This trend underscores the need for thicker or more dense materials when shielding against high-energy radiation. Upon examination of the reference value of 15 MeV pertaining to the parameters, it is observed that the zircaloy-2 sample exhibits marginally diminished values. The present study highlights a significant discovery pertaining to the superior absorption capacity of the zircaloy-2 sample. Furthermore, the study demonstrates that the zircaloy-2 sample exhibits a shorter distance between two successive interactions as compared to the zircaloy-4 and zirconium samples. Build-up factors are utilized to consider the intricate interactions between radiation particles and the atomic structure of the shielding material. The material's scattering and absorption characteristics can be ascertained as a function of the energy of the incident radiation through the provision of information. Understanding these factors is critical for accurately predicting the performance of shielding materials in real-world conditions. Through the computation of build-up factors, it is feasible to approximate the decline in radiation intensity and energy during its traversal through the shield. This information is essential for designing effective radiation protection systems that meet regulatory standards. The accuracy of this forecast holds significant importance in guaranteeing that the shielding configuration is sufficient to fulfil safety standards and protecting individuals or delicate apparatus from undue exposure to radiation. Build-up factors are employed in radiation dose computations to ascertain the radiation dose that passes through the shielding material. The precise determination of the dose is of utmost importance for the evaluation of radiation safety and adherence to regulatory norms. Incorporating

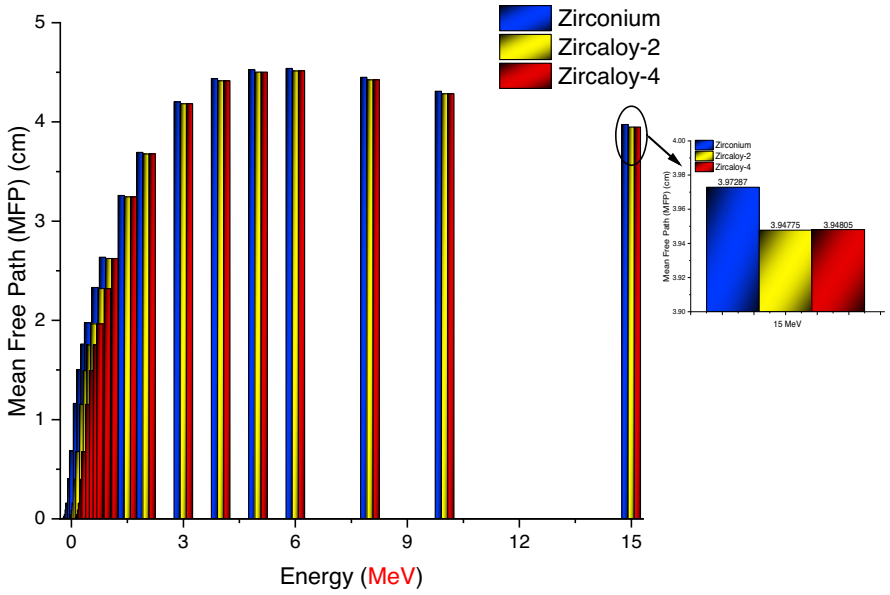

Figure 5: Variation of mean free path (cm) with photon energy (MeV) for zirconium, zircaloy-2 and zircaloy-4.

the phenomenon of build-up effect into the dose calculations enhances the accuracy and dependability of the results, thereby improving the evaluation of potential risks and the implementation of measures for radiation protection. The utilization of EBF and EABF is common in radiation shielding computations. However, they diverge in their respective representations of quantities and the information they furnish. The EBF finds its predominant application in the domains of radiation protection and dose estimations. The utilization of a shielding material is employed to approximate the degree of exposure, a crucial factor in evaluating the amount of radiation absorbed by individuals or equipment. In contrast, the EABF is frequently utilized in the fields of radiation therapy and industrial applications. The utilization of this method is aimed at computing the energy deposition within a given material, a crucial factor in the determination of the absorbed dose delivered to the target or the evaluation of the efficacy of shielding in industrial procedures. In this study, EBF and EABF values of zirconium, zircaloy-2, and zircaloy-4 samples were calculated in the range of 0.015–15 MeV and for different mean free path (mfp) values. Figures 6 and 7 show the energy-dependent changes of EBF and EABF values for different mfp values, respectively. The figures illustrate that the behavioral states of the EBF and EABF values exhibit variations based on the energy region, like the previously discussed shielding parameters. These variations underscore the importance of considering a wide range of energies when evaluating shielding materials, as different applications may expose materials to a broad spectrum of radiation energies. Upon close examination of the numerical values, it is evident that the EBF and EABF values of the zircaloy-2 sample are minimal. The data indicate that zircaloy-2 exhibits the lowest ratio between the quantities of uncollided and collided photons, signifying that the amount of uncollided photons is comparatively minimal in zircaloy-2. The aforementioned observation suggests that the photon–matter interaction in zircaloy-2 is optimized, with the structural arrangement of the material playing a significant role in facilitating the absorption process by effectively interacting with photons. This optimization could be due to

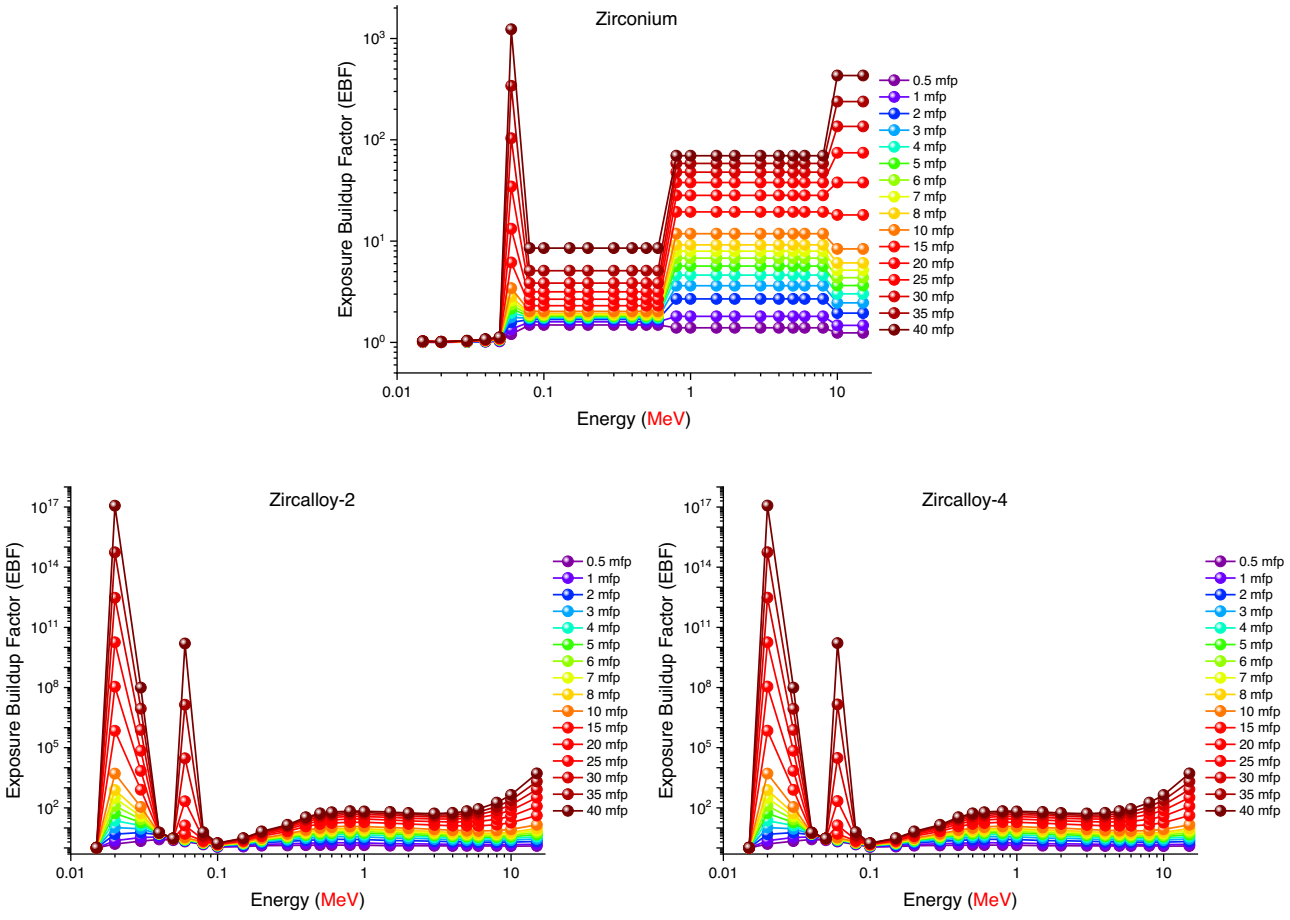

Figure 6: Variation of EBF of zirconium, zircaloy-2 and zircaloy-4 at different mean free path values.

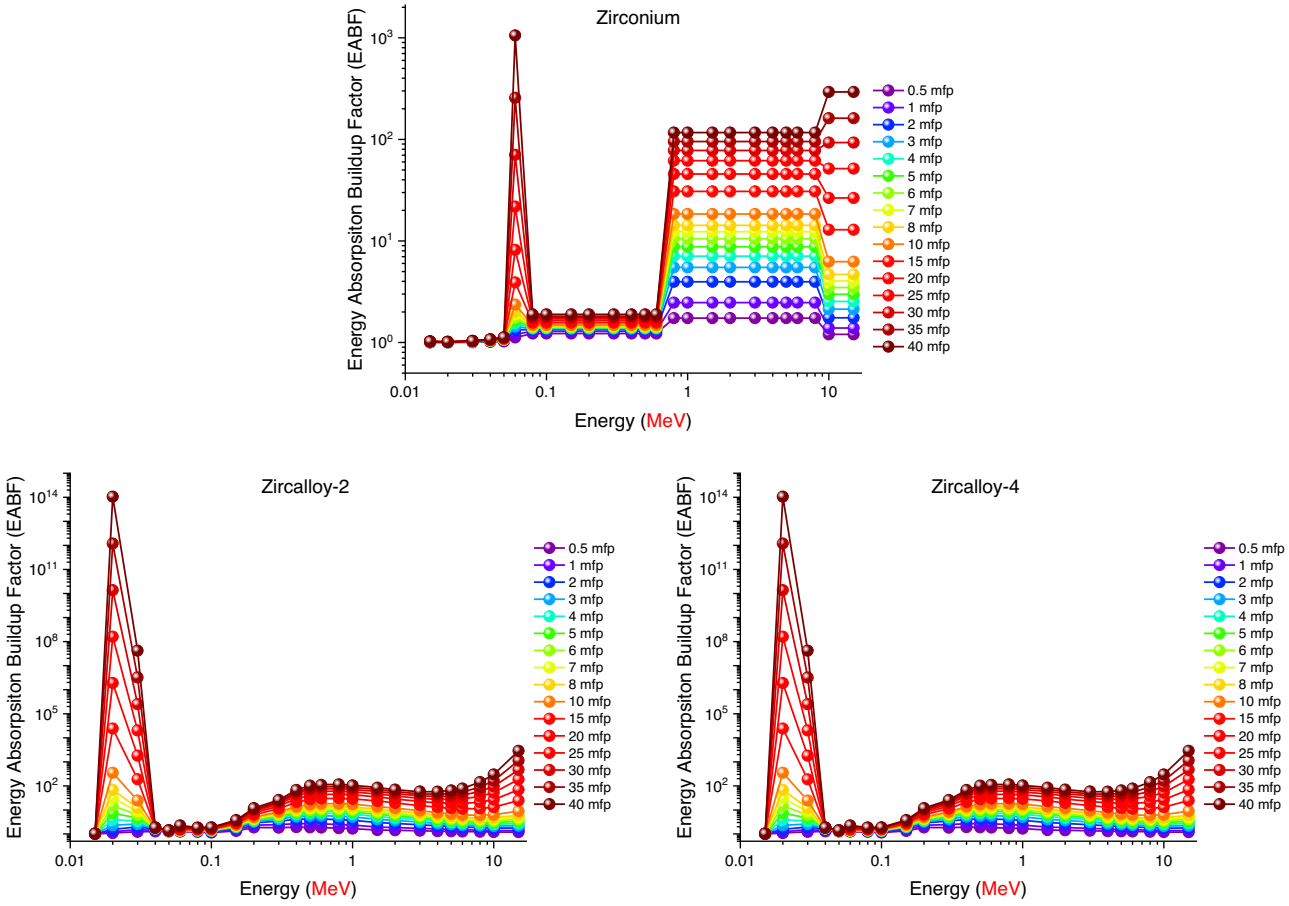

Figure 7: Variation of EABF of zirconium, zircaloy-2 and zircaloy-4 at different mean free path values.

the specific atomic arrangement and electronic structure of the alloy, which enhances photon interaction. The gamma-ray TF is a parameter utilized to ascertain the capacity of a substance to attenuate or absorb gamma rays. Through comprehension of this variable, engineers are able to make informed decisions regarding the selection of suitable shielding materials and thicknesses in order to attain the intended level of radiation mitigation. This understanding is critical for designing materials that can provide adequate protection in various radiation environments, including medical, industrial, and space applications. The current investigation involved the computation of gamma-ray transfer factors (TF) for the alloy specimens under scrutiny, utilizing Monte Carlo N-Particle code along with the ENDF/B-VII.0, MCPLIB04, EL03, and TENDL data libraries to simulate the interaction of neutrons and gamma rays with zircaloy-2 and zircaloy-4 alloys [31–36]. The present study aimed to examine the attenuation functions of primary and secondary gamma-rays within the thickness range of 0.5–3 cm for three different radioactive isotope energies, such as 0.662, 1.1732, and 1.3325 MeV. The TF values for zirconium, zircaloy-2, and zircaloy-4 at varying thicknesses and distinct radioisotope energies are depicted in Figure 8. The figure illustrates a negative correlation between TF values and zircaloy thickness, indicating a decreasing trend as the former increases. This trend highlights the increased effectiveness of thicker shielding materials in reducing gamma-ray transmission. The situation is consistent across all energy levels and can be elucidated by the proportional enhancement of gamma-ray absorption within the alloys, contingent upon the corresponding increase in material depth. The enhanced absorption in the thicker alloys resulted in a reduction of the secondary gamma-ray release from the zircaloy. This reduction is crucial for minimizing exposure to harmful secondary radiation, which can be a significant concern in radiation protection. When this decrease is compared with the primary gamma-ray quantity, the decrease in TF values becomes more understandable. Upon close examination of Figure 8, it can be observed that zircaloy-2 demonstrates the highest level of resistance to secondary gamma-ray emission and

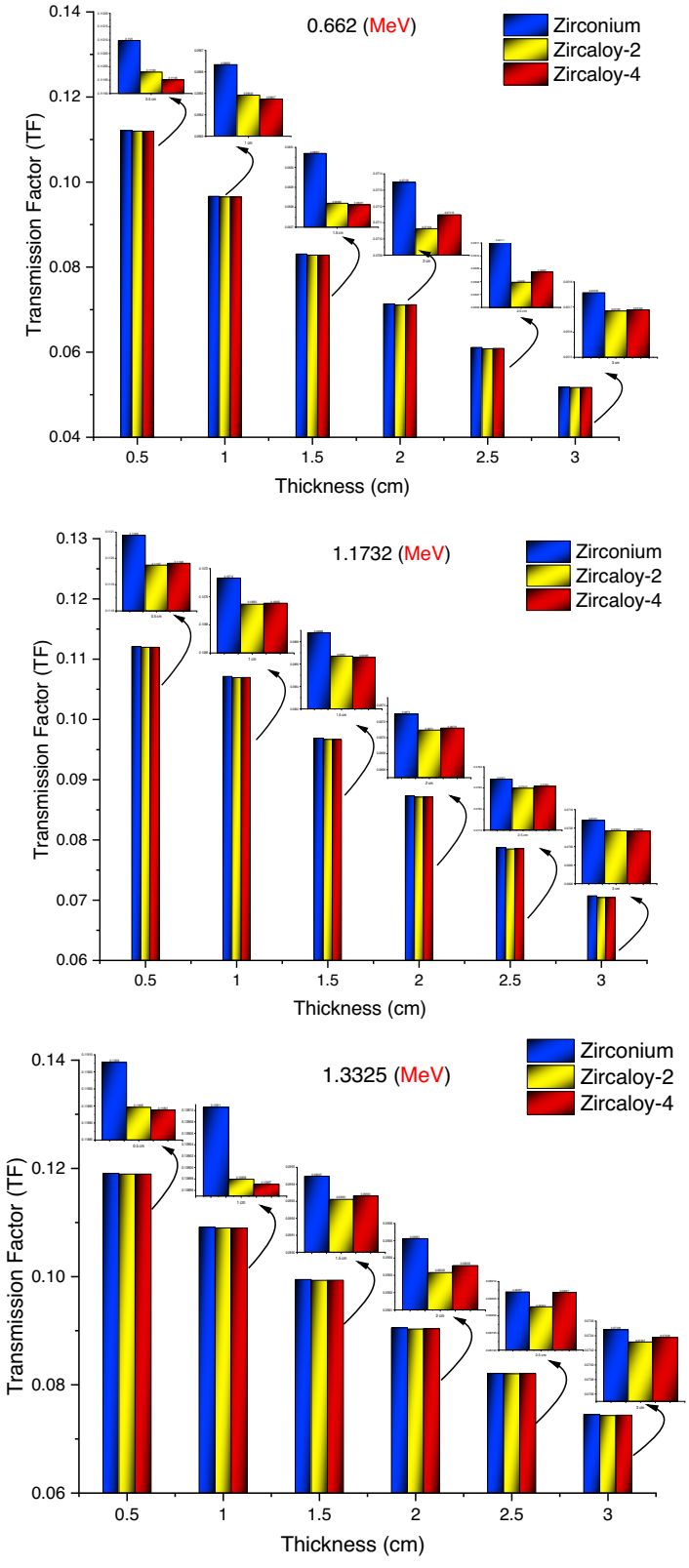

Figure 8: TFs of zirconium, zircaloy-2 and zircaloy-4 as a function of used radioisotope energy (MeV) at different glass thicknesses.

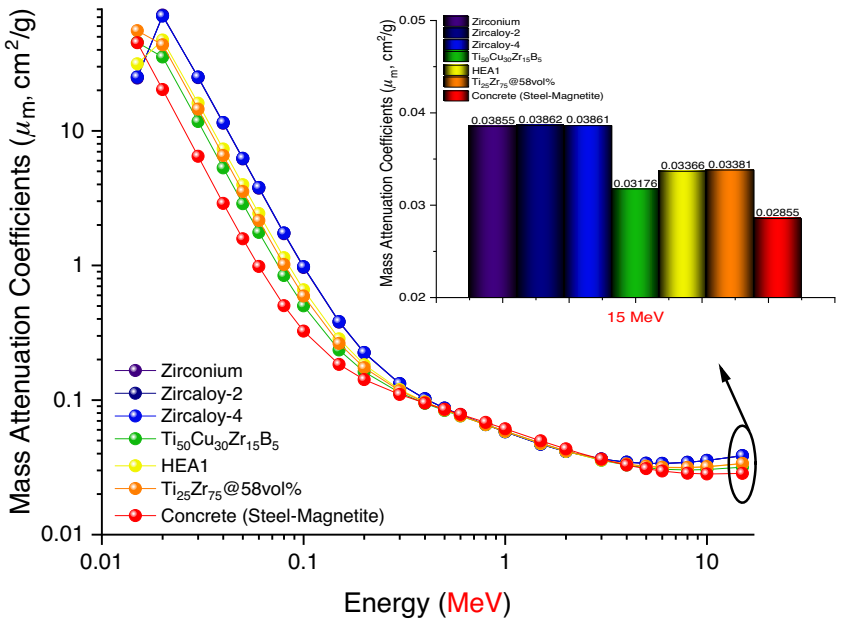

Figure 9: Comparison of MACs (μ_m, cm^2/g) for different types of alloy as a function of photon energy.

exhibits the greatest capacity for absorption. The reported outcome exhibits a high degree of consistency with the gamma-ray absorption parameters that were calculated, as well as the simulation-based TF calculations. This study compared zircaloy-2, zircaloy-4, another zirconium-based alloy, and concrete (steel-magnetite), which is often used as a shielding material. It found that zircaloy-2 had better gamma-ray attenuation properties. Figure 9 shows that the

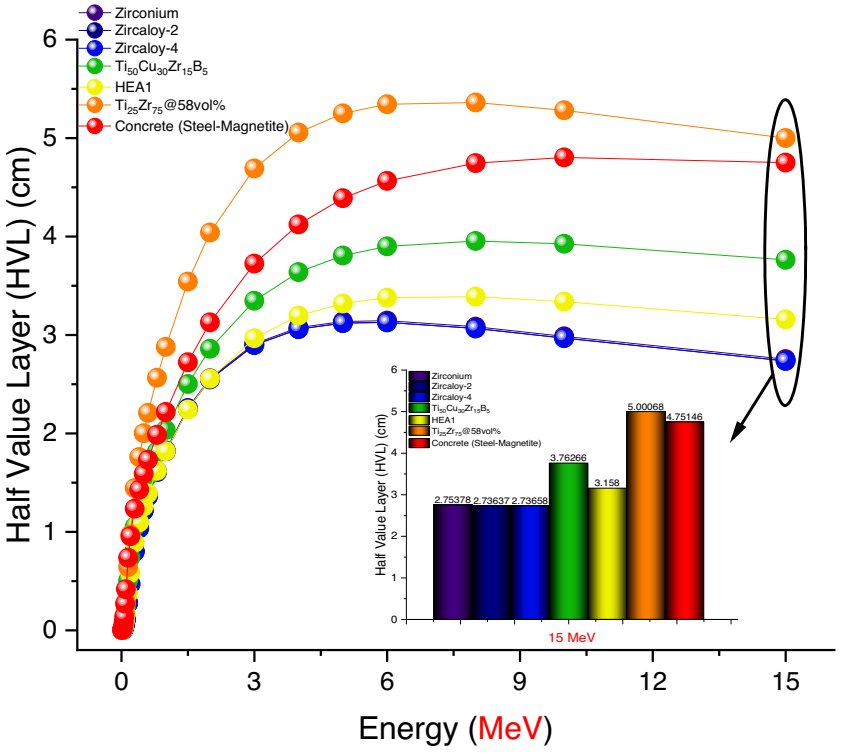

Figure 10: Comparison of half value layer (cm) for different types of alloy as a function of photon energy.

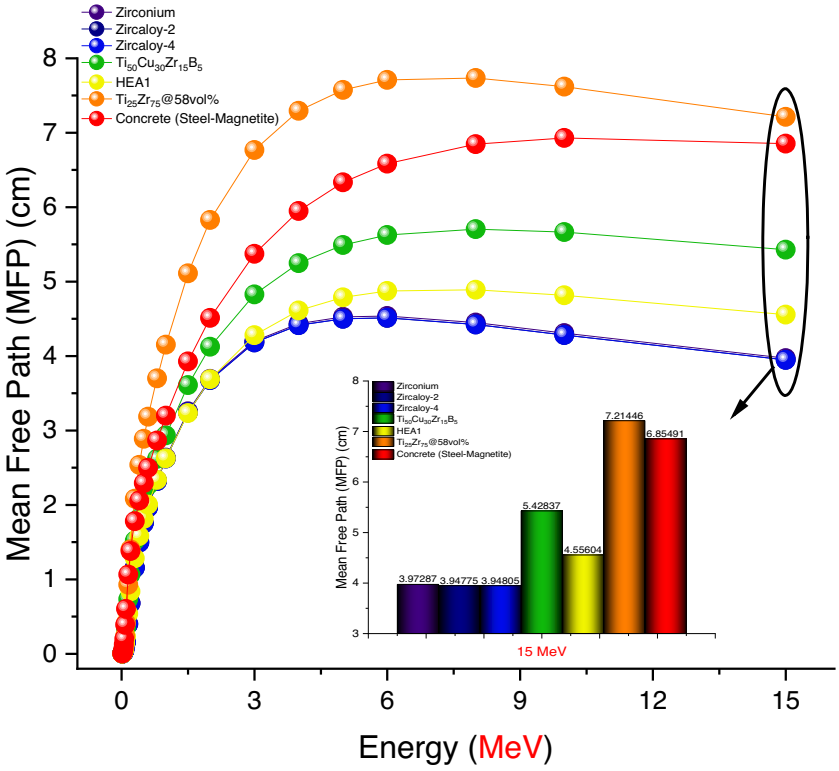

Figure 11: Comparison of mean free path (cm) for different types of alloy as a function of photon energy.

MAC for zircaloy-2 are higher than those for the other alloys and concrete that were tested [35–37]. This higher MAC value suggests that zircaloy-2 absorbs gamma rays more effectively, thereby providing better protection. The lower HVL and MFP values show that zircaloy-2 can absorb high-energy gamma rays more quickly. These rays get absorbed and neutralized more quickly, as shown in Figures 10 and 11. The lower HVL and MFP values of zircaloy-2 demonstrate that this alloy can attenuate gamma rays effectively with less material thickness.

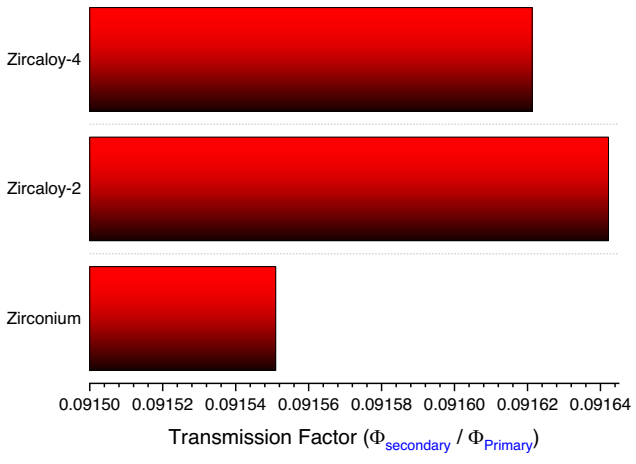

Figure 12: nTfs of zirconium, zircaloy-2, and zircaloy-4 at for 2 MeV neutrons.

3.2 Neutron attenuation properties and neutron nTFs

The primary aim of this investigation was to conduct a comparative assessment of the interaction mechanisms between zircaloy-2 and zircaloy-4 materials, two significant alloys, and gamma and neutron radiations. Hence, the TF computations illustrated in Figure 8, which were utilized for gamma rays, were similarly employed for the determination of neutron transmission factors (nTFs). This approach ensures consistency in the analysis and allows for a direct comparison between the attenuation properties of the alloys for both gamma and neutron radiations. During this phase, the F4 Tally Meshes that were previously defined remained unchanged, while the source definition underwent a redesign to accommodate 2 MeV neutrons. The input file of F4 Tally Meshes has been modified to track neutrons by redefining its output functions. This modification was necessary to accurately capture the interaction of neutrons with the alloys, which is different

from that of gamma rays. The aforementioned procedure provides that the output values derived from F4 Tally Meshes corresponded to the flux values obtained for 2 MeV neutrons. Figure 12 depicts the nTFs of zirconium, zircaloy-2, and zircaloy-4 for 2 MeV neutrons. Clearly, there exists a variation in the nTF values among the investigated alloys. These variations can be attributed to differences in the atomic composition and structure of the alloys, which affect their neutron scattering and absorption properties. Upon examination of equation (6), it becomes evident that zircaloy-2 exhibits the lowest resistance to neutron transmission among the analyzed samples. This finding suggests that zircaloy-2 does not protect against neutron radiation as well as zircaloy-4 does. This could mean that it cannot be used in places where neutron fluxes are high. The Tfn value of zircaloy-4 is 0.0218% less than that of zircaloy-2. The Tfn value of zirconium is 0.0983% less than that of zircaloy-2. The aforementioned observation suggests that zircaloy-2 exhibits a relatively low capacity for stopping neutrons. Notwithstanding the proximity of the nTF values of zircaloy-2 and zircaloy-4 alloys, computational analyses have revealed that zircaloy-2 exhibits a higher degree of neutron transition. Based on the findings of this analysis utilizing simulation techniques, zircaloy-2 decreased transition resistance in comparison to zircaloy-4. The Fast Neutron Removal Cross Section (FNRCS) measurements validate that there is a negligible disparity in neutron attenuation between zircaloy-2 and zircaloy-4. The FNRCS value for zircaloy-2 is determined to be 0.10219, but for zircaloy-4, it is measured to be 0.10221. The minor disparity suggests that both materials offer comparable neutron shielding capabilities, whereas zircaloy-2 demonstrates marginally more neutron transmission. Furthermore, the FNRCS graph presents a comparison between three different zirconium-based alloys and a widely utilized shielding material from existing literature [35–37], as depicted in Figure 13. The purpose of this comparison is to give a full picture of how well these materials work when there are a lot of neutrons present and to show how zirconium alloys stack up against a widely accepted standard for shielding.

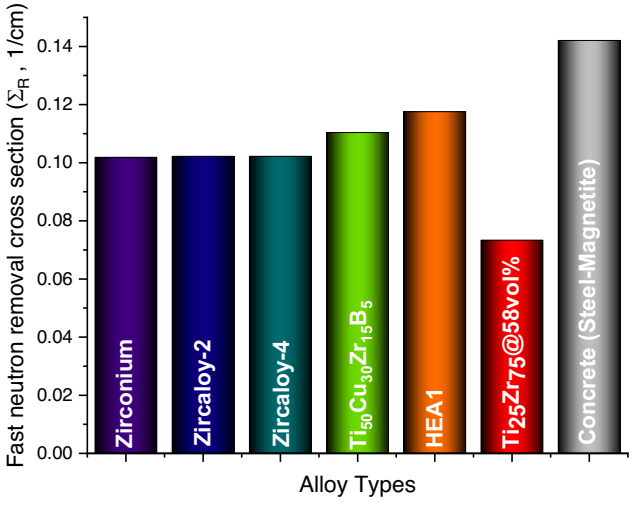

Figure 13: Variation of fast neutron removal cross section (Σ_R, 1/cm) values for different types of alloys.

4 Conclusions

Zirconium-based alloys are often used because of their advantageous material properties, including excellent corrosion resistance and high mechanical strength, making them ideal candidates for nuclear reactor components. The primary aim of this investigation was to conduct a comparative assessment of the interaction mechanisms between zircaloy-2 and zircaloy-4 materials, and gamma and neutron radiations. The TF computations, utilized for gamma rays, were similarly employed to determine nTFs. The findings of this study provide a thorough examination of the ability of zirconium alloys, specifically zircaloy-2 and zircaloy-4, to attenuate gamma-ray and neutron radiation. This detailed analysis assesses their shielding effectiveness and explores the physical mechanisms responsible for radiation attenuation. Understanding how zircaloy alloys block radiation is crucial for optimizing their use in nuclear safety applications, especially as building materials that affect system performance. Neutron and gamma-ray radiation have similar impacts on zircaloy-2 and zircaloy-4. This study arose from a lack of extensive research on zirconium alloys' ability to absorb neutrons and gamma rays under various conditions using sophisticated Monte Carlo simulations. Monte Carlo simulations offer a robust method for modeling complex interactions between radiation and materials, providing more accurate predictions of material performance under irradiation. Although zircaloy-2 and zircaloy-4 have similar mechanical capabilities, there are significant differences in their creep strengths. Creep resistance is a critical factor in determining the longevity and reliability of materials in high-temperature environments, such as nuclear reactors. Additional research is necessary to better understand the reasons behind the observed differences in neutron absorption capabilities and creep behaviors in these alloys. Based on the findings, zircaloy-2 shows excellent resilience against secondary gamma-ray emissions and has a greater ability to absorb gamma rays. This heightened absorption capacity implies possible uses in situations that demand improved

radiation shielding. The neutron nTF of zircaloy-2 and zircaloy-4 alloys are very close to each other. However, simulation results show that zircaloy-2 has slightly better neutron transmittance and suggest that zircaloy-2 has a lower susceptibility to neutron transitions compared to zircaloy-4. These findings indicate that zircaloy-2 may be less effective than zircaloy-4 as a neutron shield. This has the potential to alter the materials employed in scenarios where neutrons play a crucial role. This work provides a comprehensive analysis of the gamma and neutron radiation shielding capabilities of zircaloy-2 and zircaloy-4 alloys, making a significant contribution to the scientific literature. It also has the potential to expedite the development of materials with enhanced features for numerous applications, thereby establishing a robust foundation for future studies in this sector.

Funding information: The author states no funding involved.

Author contributions: The author has accepted responsibility for the entire content of this manuscript and approved its submission.

Conflict of interest: The author states no conflict of interest.

Data availability statement: The datasets generated during and/or analyzed during the current study are available from the corresponding author on reasonable request.

References

[1] Jaworska L, Cyboron J, Cygan S, Zwolinski A, Onderka B, Skrzekut T. Zirconium phase transformation under static high pressure and ω-Zr phase stability at high temperatures. Materials. 2019 Jul;12(14):2244. PMID: 31336839; PMCID: PMC6678209 doi: 10.3390/ma12142244.

[2] Sikka SK, Vohra YK, Chidambaram R. Omega phase in materials. Prog Mater Sci. 1982;27:245–310. doi: 10.1016/0079-6425(82)90002-0.

[3] Howell JR, Menguc MP, Daun K, Siegel R. Thermal radiation heat transfer. 7th ed. Boca Roton, Florida, USA: CRC Press; 2020. doi: 10.1201/9780429327308.

[4] Uddin MS, Chowdhury MH, Hossain SM, Latif SA, Islam MA, Hafiz MA, et al. Thermal neutron capture cross sections for the 152Sm(n,γ)153Sm and 154Sm(n,γ)155Sm reactions at 0.0536eV energy. Nucl Instrum Methods Phys Res, Sect B. 2008;266(22):4855–61. doi: 10.1016/j.nimb.2008.07.032.

[5] Karmaker N, Maraz KM, Islam F, Haque MM, Razzak M, Mollah M, et al. Fundamental characteristics and application of radiation. GSC Adv Res Rev. 2021;7(1):64–72. doi: 10.30574/gscarr.2021.7.1.0043.

[6] Zhu H, Qin M, Wei T, Davis J, Ionescu M. Atomic-scale study of He ion irradiation-induced clustering in α-Zirconium. Acta Mater. 2023;244:118584. doi: 10.1016/j.actamat.2022.118584.

[7] Gaumé M, Baldo P, Mompiou F, Onimus F. In-situ observation of an irradiation creep deformation mechanism in zirconium alloys. Scr Mater. 2018;154:87–91. doi: 10.1016/j.scriptamat.2018.05.030.

[8] Kong X, Kuang H, Li A, Yu Y, Kharchenko DO, Mao J, et al. The effect of niobium on the mechanical and thermodynamic properties of zirconium alloys. Metals. 2024;14(6):646. doi: 10.3390/met14060646.

[9] Yau TL, Annamalai VE. Corrosion of zirconium and its alloys. Ref Modul Mater Sci Mater Eng. Amsterdam, Netherlands: Elsevier; 2016. doi: 10.1016/B978-0-12-803581-8.01641-6.

[10] Jose M. Zirconia: a versatile ceramic material revolutionizing industries. Bioceram Dev Appl. 2023;13:236.

[11] Shahmiri R, Standard OC, Hart JN, Sorrell CC. Optical properties of zirconia ceramics for esthetic dental restorations: A systematic review. J Prosthet Dent. 2018;119:36–46. doi: 10.1016/j.prosdent.2017.07.009.

[12] Ernst CP, Cohnen U, Stender E, Willershausen B. In vitro retentive strength of zirconium oxide ceramic crowns using different luting agents. J Prosthet Dent. 2005;93:551–8. doi: 10.1016/j.prosdent.2005.04.011.

[13] Nigam S, McCarl L, Kumar R, Edinger RS, Kurland BF, Anderson CJ, et al. Preclinical immunopet Imaging of glioblastoma-infiltrating myeloid cells using zirconium-89 labeled Anti-CD11b antibody. Mol Imaging Biol. 2020;22(3):685–94. PMID: 31529407; PMCID: PMC7073275 doi: 10.1007/s11307-019-01427-1.

[14] AlMisned G, Sen Baykal D, Ilik E, Abuzaid M, Issa SA, Kilic G, et al. Tungsten (VI) oxide reinforced antimony glasses for radiation safety applications: A throughout investigation for determination of radiation shielding properties and transmission factors. Heliyon. 2023;9(7):e17838. doi: 10.1016/j.heliyon.2023.e17838.

[15] Khattari ZY, Al-Buriahi MS. Monte Carlo simulations and PhyX/PSD study of radiation shielding effectiveness and elastic properties of barium zinc aluminoborosilicate glasses. Radiat Phys Chem. 2022;195:110091. doi: 10.1016/j.radphyschem.2022.110091.

[16] AlMisned G, Elshami W, Rabaa E, Kilic G, Ilik E, Sen Baykal D, et al. Toward the strengthening of radioprotection during mammography examinations through transparent glass screens: A benchmarking between experimental and Monte Carlo simulation studies. Front Public Health. 2023;11:1171209. doi: 10.3389/fpubh.2023.1171209.

[17] AlMisned G, Sen Baykal D, Kilic G, Ilik E, Rabaa E, Susoy G, et al. Comparative analysis on application conditions of indium (III) oxide-reinforced glasses in nuclear waste management and source transportation: A Monte Carlo simulation study. Heliyon. 2023;9:e14274. doi: 10.1016/j.heliyon.2023.e14274.

[18] Basgoz O, Guler SH, Guler O, Canbay CA, Zakaly HM, Issa SA, et al. Synergistic effect of boron nitride and graphene nanosheets on behavioural attitudes of polyester matrix: Synthesis, experimental and Monte Carlo simulation studies. Diam Relat Mater. 2022;126:109095. doi: 10.1016/j.diamond.2022.109095.

[19] ASM Handbook Committee. Metals Handbook. Vol.2 - Properties and Selection: Nonferrous Alloys and Special-Purpose Materials. 10th ed. ASM International; 1990.

[20] Kavaz E, Tekin HO, Yorgun NY, Ozdemir O, Sayyed M. Structural and nuclear radiation shielding properties of bauxite ore doped lithium borate glasses: experimental and Monte Carlo study. Radiat Phys Chem. 2019;162:187–93. doi: 10.1016/j.radphyschem.2019.05.019.

[21] Issa SAM, Tekin HO, Erguzel TT, Susoy G. The effective contribution of PbO on nuclear shielding properties of xPbO-(100 − x)P2O5 glass system: a broad range investigation. Appl Phys A: Mater Sci Process. 2019;125:640. doi: 10.1007/s00339-019-2941-x.
[22] Al-Buriahi MS, Sriwunkum C, Arslan H, et al. Investigation of barium borate glasses for radiation shielding applications. Appl Phys A: Mater Sci Process. 2020;126:68. doi: 10.1007/s00339-019-3254-9.
[23] Kurtulus R, Kavas T, Toplan HO, Akkurt I. High-density and transparent boro-tellurite glass system against ionizing radiation: Fabrication and extensive characterization studies. Ceram Int. 2023;49(11):18455–62. doi: 10.1016/j.ceramint.2023.02.217.
[24] Yousefi M, Malidarre RB, Akkurt I, Ahmadi M, Zanganeh V. Physical, optical, mechanical, and radiation shielding properties for the B2O3-Li2O glasses. Radiat Phys Chem. 2023;209:110962. doi: 10.1016/j.radphyschem.2023.110962.
[25] Rashad M, Tekin HO, Zakaly HM, Pyshkina M, Issa SA, Susoy G. Physical and nuclear shielding properties of newly synthesized magnesium oxide and zinc oxide nanoparticles. Nucl Eng Technol. 2020;52(9):2078–84. doi: 10.1016/j.net.2020.02.013.
[26] Tekin HO, Issa SA, Kilic G, Zakaly HM, Abuzaid MM, Tarhan N, et al. In-Silico Monte Carlo Simulation Trials for Investigation of V2O5 Reinforcement Effect on Ternary Zinc Borate Glasses: Nuclear Radiation Shielding Dynamics. Mater (Basel). 2021;14:1158. doi: 10.3390/ma14051158.
[27] Tekin HO, Issa SA, Kilic G, Zakaly HM, Badawi A, Bilal G, et al. Cadmium oxide reinforced 46V2O5–46P2O5–(8− x) B2O3–xCdO semiconducting oxide glasses and resistance behaviors against ionizing gamma rays. J Mater Res Technol. 2021;13:2336–49. doi: 10.1016/j.jmrt.2021.06.020.
[28] Sing S, Kumar A, Sing D, Thind KS. Barium-borate-flyash-glasses: As radiation shielding materials. Nucl Instrum Methods Phys Res, Sect B. 2008;206:140–6. doi: 10.1016/j.nimb.2007.10.018.
[29] Kavaz E, El Agawany FI, Tekin HO, Perisanoglu U, Rammah YS. Nuclear radiation shielding using barium borosilicate glass ceramics. J Phys Chem Solids. 2020;142:109437. doi: 10.1016/j.jpcs.2020.109437.
[30] Kamislioglu M, Altunsoy Guclu EE, Tekin HO. Comparative evaluation of nuclear radiation shielding properties of xTeO$_2$ + (100–x) Li$_2$O glass system. Appl Phys A: Mater Sci Process. 2020;126:95. doi: 10.1007/s00339-020-3284-3.
[31] Alkarrani H, ALMisned G, Tekin HO. A benchmarking analysis on different rubber materials: towards customisation of lightweight and effective radiation protection solutions for aerospace and electronic applications. J Rubber Res. 2024. doi: 10.1007/s42464-024-00272-4.
[32] Chadwick MB, Obložinský P, Herman M, Greene NM, McKnight RD, Smith DL, et al. ENDF/B-VII.0: next generation evaluated nuclear data library for nuclear science and technology. Nucl Data Sheets. 2006;107(12):2931–60.
[33] Rochman D, Koning AJ. TENDL-2011: TALYS-based evaluated nuclear data library. Nuclear Research and Consultancy Group (NRG), Petten, The Netherlands. 2011.
[34] López Aldama D, Trkov A. FENDL-2.1: update of an evaluated nuclear data library for fusion applications. IAEA Report INDC (NDS)-467, International Atomic Energy Agency. 2004.
[35] Kursun C, Gao M, Guclu S, Gaylan Y, Parrey KA, Yalcin AO. Measurement on the neutron and gamma radiation shielding performance of boron-doped titanium alloy Ti50Cu30Zr15B5 via arc melting technique. Heliyon. 2023;9(11):e21696. doi: 10.1016/j.heliyon.2023.e21696.
[36] Subedi B, Paudel J, Lamichhane TR. Gamma-ray, fast neutron and ion shielding characteristics of low-density and high-entropy Mg–Al–Ti–V–Cr–Fe–Zr–Nb alloy systems using Phy-X/PSD and SRIM programs. Heliyon. 2023;9(7):e17725. doi: 10.1016/j.heliyon.2023.e17725.
[37] Okulov IV, Okulov AV, Soldatov IV, Luthringer B, Willumeit-Romer R, Wada T, et al. Open porous dealloying-based biomaterials as a novel biomaterial platform. Mater Sci Eng, C. 2018;88:95–103. doi: 10.1016/j.msec.2018.03.008.